Ion current rectification inversion in conic nanopores: Nonequilibrium ion transport biased by ion selectivity and spatial asymmetry

Yu Yan, Lin Wang, Jianming Xue, and Hsueh-Chia Chang

Additional information on J. Chem. Phys.

Ion current rectification inversion in conic nanopores: Nonequilibrium ion transport biased by ion selectivity and spatial asymmetry

Yu Yan,[1] Lin Wang,[2] Jianming Xue,[2] and Hsueh-Chia Chang[1,a)]

[1]*Department of Chemical and Biomolecular Engineering, University of Notre Dame, Notre Dame, Indiana 46556, USA*

[2]*State Key Laboratory of Nuclear Physics and Technology, School of Physics, Peking University, Beijing 100871, People's Republic of China*

We show both theoretically and experimentally that the ion-selectivity of a conic nanopore, as defined by a normalized density of the surface charge, significantly affects ion current rectification across the pore. For weakly selective negatively charged pores, intra-pore ion transport controls the current and internal ion enrichment/depletion at positive/reverse biased voltage (current enters/leaves through the tip, respectively), which is responsible for current rectification. For strongly selective negatively charged pores under positive bias, the current can be reduced by external field focusing and concentration depletion at the tip at low ionic strengths and high voltages, respectively. These external phenomena produce a rectification inversion for highly selective pores at high (low) voltage (ionic strength). With an asymptotic analysis of the intra-pore and external ion transport, we derive simple scaling laws to quantitatively capture empirical and numerical data for ion current rectification and rectification inversion of conic nanopores. © *2013 American Institute of Physics.*
[http://dx.doi.org/10.1063/1.4776216]

Ion current measurements across synthetic nanopores with surface charges, under a dc voltage bias, have revealed several surprising ion transport phenomena that clearly defy Onsager-type near-equilibrium linear response transport theories. Ion-current rectification, when the ion current is asymmetric with respect to the voltage polarization, has been observed for conic pores,[1–4] diode-like nanochannels with asymmetric charge distribution[5] and even for perfectly symmetric channels.[6] Hysteresis,[5] oscillations,[7] and "pink" current noise fluctuation[8,9] and other uniquely non-equilibrium features have been observed. Water dissociation[10,11] and vortex instabilities[12,13] have also been shown or suspected to occur at internal and external ion depleted regions, thus further revoking the linear Ohmic I-V relationship for near-equilibrium electrophoretic ion transport.

Here, we focus on an anomalous ion current feature that is unique to synthetic nanopores. While it is not surprising that bipolar pores[5] or membranes[10] can produce ion current rectification, that conic[1–4] or, more surprisingly, straight pores[6] can also exhibit current rectification remains inadequately understood. Numerical solutions of the Poisson-Nernst-Planck equation have shown that intra-pore ion depletion/enrichment plays an important role in the rectification phenomenon[14,15] and, at low external ionic strength, external ion depletion contributes to the rectification inversion.[16,17] Here, we develop a theory that delineates how intra- and external ion depletion is sensitively controlled by the ion selectivity of the pore and report experimental rectification measurements, guided by the theory, that are in quantitative agreement to the theory.

We find that, other than external ion depletion, field focusing can also play an important role in rectification inversion for conic nanopores. We verify our theory with ion current measurements through single conic nanopores. Our experimental facility and measurement techniques for polyethylene terephthalate (PET) conic nanopores and KCl solutions are described in Refs. 18 and 19.

Our theory attributes rectification and its inversion to the degree of ion selectivity of the nanopore or nanoporous membranes. In classical equilibrium membrane science, ion selectivity of a nanoporous membrane is captured by the Donnan theory, which will be paraphrased below for a cylindrical nanopore of radius R_p and arbitrary length with negative surface charge density σ_s and for a symmetric electrolyte of concentrations C_0 and valency z. Although this nanopore Donnan theory, which assumes equilibrium with the bulk, becomes invalid within the pore during non-equilibrium ion transport, it remains valid at the ends of the pore where equilibrium with the bulk is maintained at reasonable voltages. We hence develop this cylindrical nanopore equilibrium theory to derive the boundary conditions during non-equilibrium ion transport. For an electrically isolated pore without any external field penetrating the Gauss volume around the nanopore that includes the surface charge, integrating the Poisson equation over the same Gauss volume V would stipulate that the equilibrium nanopore contains no net charge or $zF \int_V (C_+ - C_-)dV = \int_V \rho \, dV = \int_{\partial V} \sigma_s \, dA$, where F is the Faraday constant and ρ the space charge density. However, another constraint is supplied by a Boltzmann equilibrium condition with the bulk electroneutral electrolyte outside the nanopore with concentration C_0, $C_\pm = C_0 \exp(\mp \frac{z\phi F}{RT})$, where R is the ideal gas constant and T the temperature. Donnan theory

a)Author to whom correspondence should be addressed. Electronic mail: hchang@nd.edu.

neglects the variation of $C_\pm$ in the transverse direction and ϕ and stipulates electroneutrality,

$$zF(C_+ - C_-) = \rho = \frac{2\sigma_s}{R_p} \qquad (1)$$

and an average intra-pore potential of $\phi = -\frac{RT}{Fz}\sinh^{-1}(\frac{\sigma_s}{C_0 R_p Fz}) = -\frac{RT}{Fz}\ln(\frac{X}{2} + \sqrt{(\frac{X}{2})^2 + 1})$. The dimensionless parameter $X = \frac{2\sigma_s}{zFC_0 R_p}$ represents the density of the surface charge, extrapolated over the entire pore volume, relative to the bulk electrolyte concentration, and is a good measure of the ion-selectivity of the pore or membrane. For weakly selective membranes with low charge density ($X \ll 1$), $\phi \sim -(RT/2zF)X$ and both ion concentrations approach the bulk value $C_\pm/C_0 \sim 1 \pm X/2$. More tellingly, for highly selective membranes ($X \gg 1$), the Donnan potential approaches $\phi \sim -(RT/zF)\ln X$ and the mobile ion concentrations $C_\pm/C_0 = \pm X/2 + \sqrt{(X/2)^2 + 1}$ approach a surface charge-controlled and bulk-independent counterion concentration of $C_+/C_0 \sim X + O(X^{-1})$ with a vanishingly small coion concentration limit $C_-/C_0 \sim 1/X + O(X^{-3})$ for the highly selective limit. A bulk independent pore conductance in the large-X limit has been experimentally verified.[20–22] Donnan theory also suggests that, at the large-X limit, the total ion concentration and the conductance of the nanopore is a universal invariance—rectification cannot occur due to change in intra-pore depletion/enrichment.[14, 16]

We expect the Donnan theory to be valid when the Debye length λ is larger than the pore size R_p and the overlapping Debye layers produce very little variation in the transverse direction. Indeed, solutions of the dimensionless equilibrium nonlinear Poisson equation for a cylindrical pore, $\frac{1}{r}\frac{d}{dr}(r\frac{d\phi}{dr}) = \eta^2 \sinh\phi$, with boundary conditions $\frac{d\phi}{dr}(r = 0) = 0$ and $\frac{d\phi}{dr}(r = 1) = -\eta^2 X/4$ and with the potential scaled by RT/zF and the radial coordinate scaled by the cylinder radius, show the area average total concentration approaches that of the Donnan theory in Fig. 1, when the ratio of the pore radius to the Debye length η is less than unity. Even if the pore radius R_p varies longitudinally, for large-X limit, the Donnan theory is still locally valid with the local R_p and equilibrium with the bulk electrolyte with concentration C_0 is sustained throughout the pore. Such an equilibrium large-X
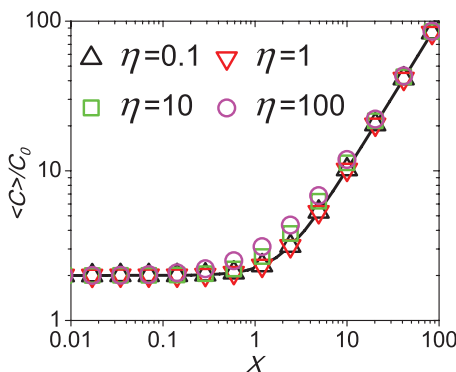

FIG. 1. Comparison of average total ionic concentration between numerical solution (symbols) and the Donnan theory (line) for a cylindrical pore at equilibrium, over a range of pore radius to Debye length ratio and X. When $X \gg 1$ or $X \ll 1$, Donnan expression is valid. For the intermediate region, the Donnan theory is less accurate as η increases.

conic pore would not exhibit rectification due to internal depletion/enrichment. A large-X conic pore at equilibrium with a symmetric bulk electrolyte, hence, has an intra-pore conductance that can be readily derived from the large-X Donnan theory by allowing for longitudinal variation[14]

$$G_{LX} = I_0/V_0 = \frac{2\pi D \sin\theta_m zF\sigma_s}{RT \ln(R_{base}/R_{tip})}, \qquad (2)$$

where D is the ionic diffusion coefficient, θ_m the half cone angle, and R_{base}, R_{tip} the base and tip radius of the cone.

However, intra-pore resistance is expected to dominate only for weakly selective nanopores ($X \ll 1$). Moreover, the Donnan theory is a near-equilibrium theory that assumes local Boltzmann equilibrium and neutrality. For a conic pore with varying cross section, the local ion selectivity increases from base to the tip as the -1 power of the local pore radius. The selectivity gradient produces ion enrichment (depletion) under positive (reverse) biased voltage when the current and dominant counterion enter (exit) the tip end. This intra-pore ion enrichment and depletion phenomena is responsible for rectification for weakly selective pores ($X \ll 1$), for which intra-pore resistance dominates the ion transport. We hence modify the near-equilibrium Donnan theory for weakly selective conic nanopores by allowing for non-equilibrium longitudinal transport.

Nevertheless, the Donnan theory remains valid at the two ends of the small-X pore, which are in equilibrium with the bulk. This is so even when the Debye layer is smaller than the pore radius R_p such that, in contrast to the assumptions made by the Donnan theory, there can be significant transverse variation in the ion distribution at the ends—all the space charge lies within the thin Debye layer on the peripheral of the pore where the counterion is in excess of the coion and much higher than its value at the pore center. We demonstrate this by carrying out the Debye-Hückel approximation at the pore ends, $C_\pm = C_0 \exp(\mp\frac{zF\phi}{RT}) \sim C_0(1 \mp \frac{zF\phi}{RT})$ in the Debye-Hückel limit with small transverse potential drop ($zF\phi/RT$) $\ll 1$. Hence, to leading order, the local averaged charge density becomes $\langle\rho\rangle = \langle C_+ - C_-\rangle \sim -(2zF/RT)C_0\langle\phi\rangle$ where $\langle\phi\rangle$ is the local cross-section averaged potential. Invoking the electroneutrality condition (Eq. (1)) and relating it to the above expression, we then obtain an invariance between the cross-section averaged potential and surface charge at the two pore ends, as constrained by electroneutrality and Boltzmann equilibrium, $\langle\phi\rangle \sim -(\frac{RT}{zF})(\frac{X}{2})$ and, to the leading order in the Debye-Hückel expansion, $\langle C_\pm\rangle/C_0 \sim 1 \pm X/2$, which are identical to the small-X Donnan theory and are without explicit dependence on the Debye length. The 6 boundary conditions for concentrations and potential at the two ends of the weakly selective (small-X) conic pore are then: $\langle C_\pm\rangle/C_0 \sim 1 \pm X/2$ for both tip and base and $\langle\phi\rangle_{tip} \sim V_0 - (\frac{RT}{zF})(\frac{X_{tip}}{2})$ while $\langle\phi\rangle_{base} \sim -(\frac{RT}{zF})(\frac{X_{base}}{2})$.

To describe the non-equilibrium intra-pore enrichment/depletion phenomena responsible for rectification of weakly selective pores, cross-section average of the Nernst-Planck transport equation can simplify the non-equilibrium transport theory. We shall derive this non-equilibrium theory for "separable" geometries like the small half angle

conic cone, whose cone surface is along the spherical radial coordinate. For such geometries, the averaging operator $\langle\rangle = \frac{1}{1-\cos\theta_m}\int_0^{\theta_m} d\theta \sin\theta$ where θ_m is the half cone angle (for small cone angle $\theta_m = \frac{R_{base}-R_{tip}}{L}$)[14,15] is independent of the radial coordinate and can hence commute with operators involving radial coordinates, thus preventing the creation of "higher moment" terms that do not correspond to the averaged concentrations. We decouple the transverse and longitudinal fields by stipulating that the longitudinal field $\frac{\partial\phi}{\partial r}$ is weaker than the transverse field, which is valid for our experiments for any applied voltage less than 10 V. As such, the potential can be decoupled into two terms, $\phi(r,\theta) \sim \phi(r) + \Phi(\theta)$. This decomposition due to field separation allows a linearization of the nonlinear longitudinal electromigration term $\langle C_\pm \frac{\partial\phi}{\partial r}\rangle \rightarrow \langle C_\pm\rangle\frac{\partial\phi}{\partial r}$ and again eliminates any problematic terms that are not the averaged concentrations. The same field separation condition also implies that we can neglect the longitudinal field to leading order at every cross section and electroneutrality condition (Eq. (1)) remains valid for the averaged charge density. The longitudinal field will enter in the averaged equation, however, and will be estimated.

Averaging the Nernst-Planck equations then produces the following two equations for the total current and ion flux in the longitudinal r direction along the conic pore:

$$\frac{J}{r^2} = -\frac{d\langle C\rangle}{dr} - \frac{\varepsilon}{r}\frac{d\phi}{dr}, \tag{3a}$$

$$\frac{I}{r^2} = \frac{\varepsilon}{r^2} - \langle C\rangle\frac{d\phi}{dr}, \tag{3b}$$

where $\langle C\rangle = \langle C_+\rangle + \langle C_-\rangle$, and the averaged charged density $\langle\rho\rangle$ has been replaced by the electroneutrality condition (Eq. (1)). The characteristic properties for scaling are the bulk concentration C_0, the pore length L, the characteristic flux density DC_0/L, ion flux and current by $2\pi Fz(1-\cos\theta_m)DC_0L$, and the thermal potential RT/zF. With this scaling, the tip and base, where the derived boundary conditions are imposed, are located at $r_1 = \frac{R_{tip}}{R_{base}-R_{tip}}$ and $r_2 = \frac{R_{base}}{R_{base}-R_{tip}}$. The small parameter is $\varepsilon = \frac{\sin\theta_m}{2(1-\cos\theta_m)}X_{tip}\frac{R_{tip}}{L}$ (for small half cone angle, $\varepsilon = X_{tip}\frac{R_{tip}}{R_{base}-R_{tip}}$) where X_{tip} is evaluated with the tip radius. This small parameter is about the same order as X evaluated at R_{base}. The averaged flux equations (Eq. (3)) with the unknown total current I and ion flux J must be solved with the 6 derived boundary conditions.

Using a simple ansatz for the averaged concentration $\langle C\rangle = \langle C\rangle_0 + \varepsilon\langle C\rangle_1 + \cdots$, the potential and the fluxes, one obtains the near-equilibrium Ohmic electromigration equations without surface charge effect and with homogeneous concentration—with uniform conductivity within the pore, $\frac{J_0}{r^2} = -\frac{d\langle C\rangle_0}{dr}$ and $\frac{I_0}{r^2} = -\langle C\rangle_0\frac{d\phi_0}{dr}$. Using the leading order boundary condition $\langle C\rangle_0 = 2$ for both tip and base and $\phi_{0tip} = V_0$ while $\phi_{0base} = 0$, one then obtains the Ohmic solution with homogeneous ionic strength $\langle C\rangle_0 = 2$ and its longitudinal potential distribution $\phi_0 = \frac{V_0 r_1(r_2-r)}{r}$. This potential distribution then yields the dimensionless version effective conductance of an Ohmic pore without surface charge $I_0/V_0 = 2r_1r_2$, which yields the dimensional weak selectivity (small-X) conductance after multiplying by

$$\frac{2\pi F^2z^2(1-\cos\theta_m)DC_0L}{RT}$$

$$G_{SX} = \frac{4\pi F^2z^2(1-\cos\theta_m)DC_0LR_{tip}R_{base}}{RT(R_{base}-R_{tip})^2}$$

$$= \frac{2\pi F^2z^2DC_0R_{tip}R_{base}}{RTL} \tag{4}$$

that augments the large-X cone Ohmic conductance in Eq. (2).

In the next order, however, the surface charge effect becomes important and the resulting selectivity gradient is responsible for the internal depletion and enrichment, $\frac{J_1}{r^2} = -\frac{d\langle C\rangle_1}{dr} - \frac{1}{r}\frac{d\phi_0}{dr}$ and $\frac{I_1}{r^2} = \frac{1}{r^2} - \langle C\rangle_0\frac{d\phi_1}{dr} - \langle C\rangle_1\frac{d\phi_0}{dr}$. Imposing the next order boundary conditions $\langle C\rangle_1 = 0$ and $\phi_1 = -\frac{1}{2r}$ for both tip and base then yields

$$\langle C\rangle_1 = \frac{V_0(r_2-r)(r-r_1)}{2r^2}. \tag{5}$$

Since $r_1 \leq r \leq r_2$, the sign of this ionic strength correction term to the near-equilibrium homogenous ion concentration distribution, $\langle C\rangle_0 = 2$, and whether internal depletion or enrichment occurs is then governed by the voltage bias, the sign of V_0. This estimate of enrichment and depletion profile is in good agreement with numerical solution of the Poisson-Nernst-Planck equation for a weakly selective conic pore, as seen in Fig. 2(a). Here, the 1D simulation is carried out by solving the averaged Poisson-Nernst-Planck with Donnan theory as boundary conditions at the tip and base,[14,15] while in the 2D simulation the full Poisson-Nernst-Planck for 2D symmetric cone with two large reservoirs is used.[4] The current correction from the Ohmic current is $I_1 = \frac{V_0^2}{12}$ and one hence gets a simple estimate for the incremental current and the rectification factor as small-X, $Rf - 1 \sim \frac{I_+}{I_-} - 1 = \frac{\varepsilon V_0}{12r_2r_1}$, or in dimensional form

$$\frac{12(Rf-1)R_{base}R_{tip}}{(R_{base}-R_{tip})^2} = \Sigma \sim \frac{\varepsilon FzV_0}{RT} = \frac{2\sigma_s V_0}{RTC_0(R_{base}-R_{tip})}, \tag{6}$$
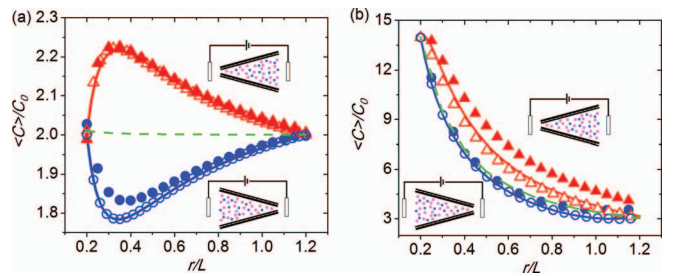

FIG. 2. Comparison of theory (lines) to computed enrichment and depletion profiles (symbols) for weakly and strongly selective conic pores with opposite polarization at $FV/RT = 10$. The total concentration for Donnan equilibrium (green dashes), namely, when $V = 0$, is also given for comparison. The computation is done by solving both 1D (open symbol) and 2D (closed symbol) Poisson-Nernst-Planck equations. Enrichment occurs when applying a voltage from tip to base (positive V_0, red, lines and up triangles) and depletion with reverse bias (blue, lines and circles). The tip radius, base radius, length, and surface charge density of nanopore are fixed at 5 nm, 30 nm, 1 μm and 0.05 C/m^2, respectively. The size of the reservoirs for 2D is 500 nm × 500 nm. A symmetric electrolyte KCl with the diffusion coefficient of 2×10^{-9} m^2/s is used. (a) Weakly selective, the concentration is 1000 mM ($X_{tip} = 0.21$). (b) Strongly selective, the concentration is 15 mM ($X_{tip} = 13.8$).
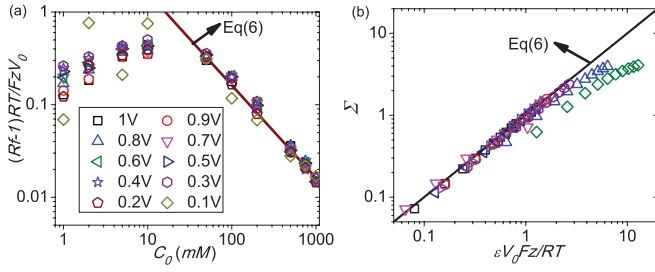
FIG. 3. (a) Collapse of measured rectification factor data for 12 μm PET nanopore, with a tip radius of 19 nm and base 268 nm, surface charge 0.19 C/m^2 (estimated from 1M data) by our small-X theory (line). (b) Collapse of 2D numerical rectification data for different geometries plus simulation data from literature[23] (magenta down triangle) with surface charge ranging from 0.00625 to 0.2 e/nm^2 and bulk concentration from 0.25 M to 2 M. The simulation parameters (tip radius-base radius-length-surface charge-concentration) are: 5 nm-30 nm-1 μm-0.05 C/m^2-2000 mM (black square), 5 nm-30 nm-1 μm-0.05 C/m^2-1000 mM (red circle), 5 nm-30 nm-1 μm-0.05 C/m^2-250 mM (blue up triangle), 5 nm-30 nm-1 μm-0.1 C/m^2-250 mM (olive diamond), 5 nm-30 nm-1 μm-0.01 C/m^2-250 mM (navy left triangle), 3 nm-30 nm-1 μm-0.05 C/m^2-1000 mM (violet right triangle) and 15 nm-30 nm-1 μm-0.05 C/m^2-1000 mM (purple hexagon), respectively.

which is in good agreement with both numerical and experimental data in the small-X limit, as seen in Fig. 3. The numerical data include ones reported in the literature[23] as well as our own and the normalization involves raw parameters.

Similarly, a perturbation around large-X limit can be done for intra-pore ion transport after introducing the small parameter $\delta \sim \frac{1}{\epsilon}$. Use the same characteristic scaling and scale $C_\delta = C\delta$, $J_\delta = J\delta$, $I_\delta = I\delta$. The 6 new dimensionless boundaries for large-X conic pore are: $\langle C_\delta \rangle \sim \delta(X + \frac{2}{X})$ $= \frac{1}{r} + 2\delta^2 r$ for both tip and base and $\phi_{tip} \sim V_0 - (\ln \frac{1}{\delta r_{tip}}$ $+ \delta^2 r_{tip}^2)$ while $\phi_{base} \sim -(\ln \frac{1}{\delta r_{base}} + \delta^2 r_{base}^2)$. For the leading order, $\frac{J_{\delta 0}}{r^2} = -\frac{d\langle C_\delta \rangle_0}{dr} - \frac{1}{r}\frac{d\phi_0}{dr}$ and $\frac{I_{\delta 0}}{r^2} = \frac{1}{r^2} - \langle C_\delta \rangle_0 \frac{d\phi_0}{dr}$, together with the leading boundary conditions, the total concentration is $\langle C_\delta \rangle_0 = \frac{1}{r}$ and the conductance is I_0/V_0 $= I_{\delta 0}/\delta V_0 = \frac{1}{\delta \ln(r_2/r_1)}$, which is identical to the equilibrium large-X conductance (Eq. (2)) after multiplying by the scaling factor $\frac{2\pi F^2 z^2 (1-\cos\theta_m) D C_0 L}{RT}$. The next order is trivial as the boundary condition does not explicit contain $O(\delta)$. For the $O(\delta^2)$ order that corrects this equilibrium conductance, one obtains

$$\frac{J_{\delta 2}}{r^2} = -\frac{d\langle C_\delta \rangle_2}{dr} - \frac{1}{r}\frac{d\phi_2}{dr}, \tag{7a}$$

$$\frac{I_{\delta 2}}{r^2} = -\langle C_\delta \rangle_0 \frac{d\phi_2}{dr} - \langle C_\delta \rangle_2 \frac{d\phi_0}{dr}. \tag{7b}$$

Imposing the boundary condition $\langle C_\delta \rangle_2 = 2r$ and $\phi_2 \sim -r^2$ at the tip and base, the intra-pore concentration correction at large-X is found to be related to the equilibrium current $I_{\delta 0}$ by

$$\langle C_\delta \rangle_2 = \frac{2(r_1^2 - r_2^2)}{r_1^{2-I_{\delta 0}} - r_2^{2-I_{\delta 0}}} r^{1-I_{\delta 0}} + \frac{2(r_1^{I_{\delta 0}} - r_2^{I_{\delta 0}})}{r_1^{I_{\delta 0}-2} - r_2^{I_{\delta 0}-2}} r^{-1}. \tag{8}$$

Figure 2(b) shows the enrichment still occurs at forward bias and depletion at backward bias. The current correction hence
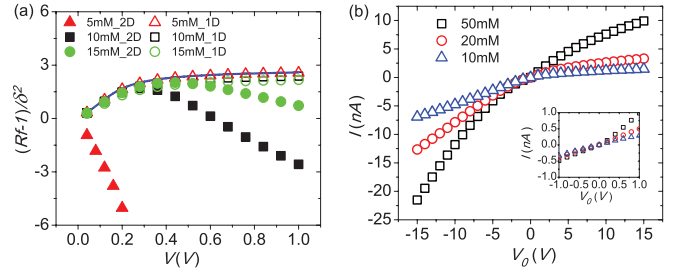

FIG. 4. A nanopore with a tip radius of 5 nm, base radius 30 nm, length 1 μm and surface charge 0.05 C/m^2 is used. (a) Comparison of large-X intra-pore rectification theory (line) of Eqs. (9) and (10) to computed rectification factor (symbols) at various voltage and concentration. The computation is done by solving both 1D (open symbol, no external region) and 2D (closed symbol, with external region) Poisson-Nernst-Planck equations. Deviation from the theory occurs at large voltage and low concentration (for 2D) when external depletion occurs and the rectification inverts with negative $(Rf - 1)$. Away from these conditions, the rectification factor approaches constant at large voltages, as predicted by Eq. (10). (b) 2D numerical I-V curves showing opposite rectification at low (inset) and high voltages.

will be

$$I_{\delta 2} = \frac{I_{\delta 0}(r_1^2 - r_2^2)}{\ln(r_2/r_1)(I_{\delta 0} - 2)} + \frac{2(I_{\delta 0} - 1)(r_1^{I_{\delta 0}} - r_2^{I_{\delta 0}})}{r_1^{I_{\delta 0}-2} - r_2^{I_{\delta 0}-2}}. \tag{9}$$

At high voltage when $|I_{\delta 0}| \gg 1$ and when the conic pore is sharp ($r_1 \ll r_2$), this correction current approaches a constant $I_{\delta 2} = \{ \frac{(r_1^2-r_2^2)}{\ln(r_2/r_1)} + \frac{2r_2^2 I_{\delta 0}(I_{\delta 0}>0)}{2r_1^2 I_{\delta 0}(I_{\delta 0}<0)}$, as shown in Fig. 4(a), with a constant rectification factor $Rf - 1 \sim 2\delta^2(r_2^2 - r_1^2)$ for $|I_{\delta 0}| \gg 1$ or in dimension form

$$Rf - 1 \sim 2\frac{(R_{base}^2 - R_{tip}^2)}{X_{tip}^2 R_{tip}^2}. \tag{10}$$

Figure 4(a) shows this predicted rectification factor from the large-X intra-pore ion current theory for highly selective pores collapses the 1D numerical model (without external region). As is consistent with the theory, $Rf - 1$ has a C^{-2} dependence on the concentration and approaches a voltage-independent asymptote for large voltage. For positive bias V_0, both the small-X intra-pore theory (Eq. (6)) and the large-X intra-pore theory (Eqs. (9) and (10)) predict a positive rectification factor $Rf - 1$, suggesting that intra-pore theory cannot account for rectification inversion at large X. However, with the increase of voltage or decrease of concentration, the 2D model (with external region) starts to deviate from the large-X intra-pore theory and 1D model. This deviation indicates that external region plays an important role under these limiting conditions and is responsible for rectification inversion. Figure 4(a) also shows rectification inversion, when $Rf - 1$ becomes negative, at low concentrations and high voltages for the 2D model. This rectification inversion phenomenon occurs at diminishing voltages as X increases (or ionic strength decreases, also see Fig. 4(b)), until the critical voltage vanishes at a critical X in Fig. 4(a). This suggests that beyond a critical X, external resistance becomes so dominant that the intra-pore theory of Eqs. (9) and (10) becomes invalid. Hence, at a sufficiently large X, the rate-limiting step for ion transport is no longer intra-pore ion transport but rather

external resistance. Since the rectification inversion phenomenon is defined relative to the intra-pore rectification theory, inversion may occur at zero voltage when X exceeds a critical value.

It has been shown numerically[16] and experimentally[6,12,13] that, at higher voltages, external concentration depletion and enrichment begin to develop at the pore entrance (where counterion and current enter) and exit, respectively, of any weakly or strongly selective nanopores or nanoporous membranes. A limiting current occurs beyond a critical voltage when the ion concentration at the pore entrance (membrane surface) becomes zero at the depletion end and, for small cylindrical pores, the ions within a roughly spherical external region (with a radius comparable to the pore radius) is severely depleted. Since intra-pore enrichment occurs with positive bias when the current enters the tip, we then expect external resistance due to ion depletion at the tip can invert the rectification phenomenon beyond a critical voltage corresponding to the onset of the limiting current. However, we shall show another phenomenon, field focusing as described by the classical Hall resistance of ion flux into a pore, also plays a role in the rectification inversion and is responsible for the critical X observed in Fig. 4.

With the radial symmetry of the external concentration and electric fields, we can model the external depletion phenomenon with a pseudo-one-dimensional model with radial symmetry. Since intra-pore ion transport is unimportant when external depletion occurs and becomes the bottle neck for ion transport, we can assume the pore is an ideally selective cylindrical pore with radius R_p corresponding to the radius at one end of the pore (R_{base} or R_{tip}) where the counterion enters the pore (where depletion occurs). This cylindrical pore is connected coaxially to a much bigger hemispherical reservoir (radius L_r), with electrodes on the sphere surface and a symmetric electrolyte of concentration C_0. For symmetric electrolytes that are electroneutral, $C_+ = C_- = C$, the electromigration flux into the ideally selective cylindrical pore is exactly equal to the diffusive flux[21] and the Nernst-Planck equation for the ions reduce the diffusion equation, $\frac{1}{r^2}\frac{d}{dr}(r^2\frac{dC}{dr}) = 0$ with two boundary conditions $C = (C_0, 0)$ at $r = (L_r, R_p)$, respectively, at limiting-current conditions. The concentration profile at limiting-current for this radially symmetric depletion region is then $C = C_0(\frac{L_r}{L_r - R_p} - \frac{R_p L_r}{L_r - R_p}\frac{1}{r})$ and limiting current is $I = J = zF2D\frac{dC}{dr}2\pi r^2 = 4\pi zFDC_0\frac{L_r R_p}{L_r - R_p} \sim 4\pi zFDC_0 R_p$. For highly selective conic pores with a positive applied bias from tip to base is then $I_{\lim} = 4Fz\pi DC_0 R_{tip}$.[21]

Figure 5(a) shows the resistance of large-X pore increases after the current exceeds this limiting current, with a large decrease in the current. The large increase in external resistance at the tip beyond the onset of limiting current overwhelms the decrease in intra-pore resistance under positive voltage bias, thus inverting the rectification. The limiting voltage when the limiting current occurs is, hence, a good criterion for the rectification inversion. A good estimate of the rectification inversion voltage can then be obtained by combining the intra-pore resistance from our large-X theory in Eq. (2) with the large-X limiting current due to external depletion to yield the limiting-
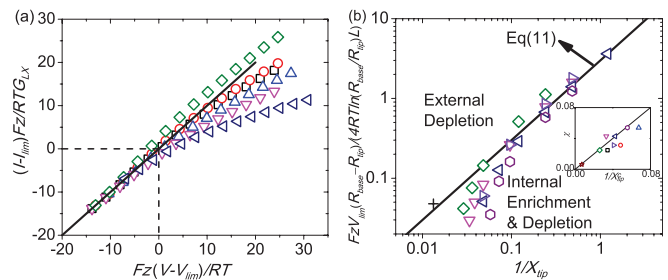

FIG. 5. (a) 2D numerical results (positive bias) for large-X indicating limiting current or voltage as a hallmark for the deviation from the case without external depletion (line). The resistance increases after the voltage exceeds limiting voltage. The simulation parameters (tip radius-base radius-length-surface charge-concentration) are: 5 nm-30 nm-1 μm-0.05 C/m^2-10 mM (black square), 2.5 nm-30 nm-1 μm-0.05 C/m^2-15 mM (red circle), 5 nm-30 nm-0.5 μm-0.05 C/m^2-15 mM (blue up triangle), 5 nm-30 nm-1 μm-0.01 C/m^2-2 mM (magenta down triangle), 5 nm-60 nm-1 μm-0.05 C/m^2-15 mM (olive diamond) and 5 nm-30 nm-1 μm-0.05 C/m^2-5 mM (navy left triangle), respectively. (b) Collapse of 2D numerical results of rectification inversion voltage as a function of X scaling with an empirical factor of 3. One data point (black cross is from literature[23]). There exists a critical $1/X_{tip}^c$ below which rectification inversion happens right away. The inset shows collapse of the numerical data for the critical X_{tip}^c by a theory based on Hall resistance due to field focusing. The simulation parameters (tip radius-base radius-length-surface charge) are: 2.5 nm-30 nm-1 μm-0.01 C/m^2 (black square), 5 nm-60 nm-1 μm-0.01 C/m^2 (red circle), 5 nm-30 nm-0.5 μm-0.01 C/m^2 (blue up triangle), 5 nm-30 nm-1 μm-0.05 C/m^2 (magenta down triangle), 2.5 nm-30 nm-1 μm-0.05 C/m^2 (olive diamond), 5 nm-30 nm-0.01 C/m^2 (navy left triangle), 5 nm-60 nm-1 μm-0.05 C/m^2 (violet right triangle), 5 nm-30 nm-0.5 μm-0.05 C/m^2 (purple hexagon) and 4 nm-250 nm-12 μm-0.08 C/m^2 (wine star), respectively.

voltage

$$\frac{V_{\lim} Fz}{RT} = \frac{4\ln(R_{base}/R_{tip})L}{(R_{base} - R_{tip})X_{tip}}. \tag{11}$$

This prediction is favorably compared to our and literature numerical rectification inversion voltage at large-X, as seen in Fig. 5(b). An empirical factor of 3 is used to obtain quantitative collapse of the data. This factor of 3 is probably due to the fact that the concentration at the pore entrance is not exactly zero, as is assumed in our limiting current estimate. As predicted, the rectification inversion voltage blows up as -1 power of X, as X approaches zero, but the theory fails to predict a critical X beyond which rectification inversion occurs at zero voltage, which was first seen in Fig. 4(a).

This critical X arises because, at very large-X, field focusing effect or Hall resistance,[24,25] which exists for both polarizations but can offset the intra-pore enrichment at positive bias (lower concentration at tip) so that intra-pore rectification fails to develop. Mathematically, the derivation for field focusing effect is analogous to limiting current, since the Laplace equation describes both the potential distribution for field focusing and concentration distribution for limiting current. With the same geometric model above, the potential satisfies $\frac{1}{r^2}\frac{d}{dr}(r^2\frac{d\varphi}{dr}) = 0$ with two boundary conditions $\varphi = (V_0, 0)$ at $r = (L_r, R_p)$. So the dimension conductance for the reservoir is $I_0/V_0 = zFzF\frac{D}{RT}2C_0\frac{d\varphi}{dr}2\pi r^2/V_0 = 4\pi zFDC_0 R_p\frac{zF}{RT} = I_{\lim}\frac{zF}{RT}$. This simple derivation of the Hall resistance is off by a factor $\pi/2$ from the literature value[24] $R_{Hall} = \frac{RT}{8z^2F^2DC_0R_p}$, which was derived by correcting the

radial symmetry with a more detailed analysis in a hemispherical neighborhood of radius R_p near the entrance. Despite the mathematical similarity, the physical mechanism for the Hall field focusing phenomenon at the entrance is quite distinct from the limiting current due to tip ion depletion. We hence match the higher order large-X intra-pore conductance, corresponding to the leading order large-X intra-pore conductance (Eq. (2)) multiplied by the higher-order intra-pore rectification factor (Eq. (10)), with the inverse Hall resistance to obtain a condition for the critical X beyond which field focusing Hall effect towards the tip is as important as external ion depletion at the tip as the dominant process in ion transport,

$$\frac{1}{X_{tip}^c} = \chi = \left(\frac{\pi R_{tip}^2}{16 \ln(R_{base}/R_{tip}) L(R_{base} + R_{tip})} \right)^{1/3}.$$
(12)

This estimate is seen in the inset of Fig. 5(b) to capture the numerical values for the critical X above which rectification inversion at zero voltage—when the intra-pore rectification is not observed. Below this critical X, inversion is due only to external depletion and the rectification inversion voltage is predicted by Eq. (11).

Our attempts to measure this rectification inversion voltage at low concentrations with our conic nanopores encountered severe current instabilities which did not allow us to obtain reliable current data or rectification inversion concentrations. We did, however, observe rectification inversion at high voltages and low ionic strengths as is qualitatively consistent with the theory.

In summary, we report a perturbation theory (confirmed by experimental measurement and numerical simulation) that explains the rectification phenomenon for weakly (small-X) and highly selective (large-X) conic pores. The former is due to intra-pore enrichment and depletion that results from ion selectivity gradient introduced by the conic geometry. The rectification of highly selective nanopores at high voltage is due, instead, to external concentration depletion at the end where the counterion and current enters the pore. Its rectification direction is opposite from the weakly selective nanopore, thus producing a rectification inversion phenomenon at high voltages. Another rectification inversion mechanism is identified at low concentrations due to field focusing Hall effect amplified by external ion depletion such that, beyond a critical X, the rectification inversion occurs at zero voltage—the intrapore ionic transport is unimportant for all voltages. Quantitative predictions of the rectification factor and rectification inversion voltages and concentrations are favorably compared to numerical and experimental data.

[1] Z. Siwy and A. Fuliński, Phys. Rev. Lett. **89**, 198103 (2002).
[2] C. Wei, A. J. Bard, and S. W. Feldberg, Anal. Chem. **69**, 4627 (1997).
[3] Z. Siwy, E. Heins, C. C. Harrell, P. Kohli, and C. R. Martin, J. Am. Chem. Soc. **126**, 10850 (2004).
[4] X. Wang, J. Xue, L. Wang, W. Guo, W. Zhang, Y. Wang, Q. Liu, H. Ji, and Q. Ouyang, J. Phys. D: Appl. Phys. **40**, 7077 (2007).
[5] L.-J. Cheng and L. J. Guo, ACS Nano **3**, 575 (2009).
[6] G. Yossifon, Y.-C. Chang, and H.-C. Chang, Phys. Rev. Lett. **103**, 154502 (2009).
[7] M. R. Powell, M. Sullivan, I. Vlassiouk, D. Constantin, O. Sudre, C. C. Martens, R. S. Eisenberg, and Z. S. Siwy, Nat. Nanotechnol. **3**, 51 (2008).
[8] S. Howorka and Z. Siwy, Chem. Soc. Rev. **38**, 2360 (2009).
[9] C. Tasserit, A. Koutsioubas, D. Lairez, G. Zalczer, and M.-C. Clochard, Phys. Rev. Lett. **105**, 260602 (2010).
[10] L.-J. Cheng and H.-C. Chang, Biomicrofluidics **5**, 046502 (2011).
[11] M. B. Andersen, M. van Soestbergen, A. Mani, H. Bruus, P. M. Biesheuvel, and M. Z. Bazant, Phys. Rev. Lett. **109**, 108301 (2012).
[12] S. M. Rubinstein, G. Manukyan, A. Staicu, I. Rubinstein, B. Zaltzman, R. G. H. Lammertink, F. Mugele, and M. Wessling, Phys. Rev. Lett. **101**, 236101 (2008).
[13] G. Yossifon and H.-C. Chang, Phys. Rev. Lett. **101**, 254501 (2008).
[14] J. Cervera, B. Schiedt, R. Neumann, S. Mafe, and P. Ramirez, J. Chem. Phys. **124**, 104706 (2006).
[15] J. Cervera, A. Alcaraz, B. Schiedt, R. Neumann, and P. Ramirez, J. Phys. Chem. C **111**, 12265 (2007).
[16] D. Momotenko, F. Cortes-Salazar, J. Josserand, S. Liu, Y. Shao, and H. H. Girault, Phys. Chem. Chem. Phys. **13**, 5430 (2011).
[17] Y. Ai, M. Zhang, S. W. Joo, M. A. Cheney, and S. Qian, J. Phys. Chem. C **114**, 3883 (2010).
[18] J. Xue, Y. Xie, Y. Yan, J. Ke, and Y. Wang, Biomicrofluidics **3**, 022408 (2009).
[19] L. Wang, Y. Yan, Y. Xie, L. Chen, J. Xue, S. Yan, and Y. Wang, Phys. Chem. Chem. Phys. **13**, 576 (2011).
[20] D. Stein, M. Kruithof, and C. Dekker, Phys. Rev. Lett. **93**, 035901 (2004).
[21] G. Yossifon, P. Mushenheim, Y.-C. Chang, and H.-C. Chang, Phys. Rev. E **79**, 046305 (2009).
[22] H.-C. Chang and L. Y. Yeo, *Electrokinetically Driven Microfluidics and Nanofluidics* (Cambridge University Press, 2009), Chap. 2.
[23] I. Vlassiouk, T. R. Kozel, and Z. S. Siwy, J. Am. Chem. Soc. **131**, 8211 (2009).
[24] J. Hall, J. Gen. Physiol. **66**, 531 (1975).
[25] I. Vlassiouk, S. Smirnov, and Z. Siwy, Nano Lett. **8**, 1978 (2008).